$I = 0$ $C = +1$ mesons from 1920 to 2410 MeV

A.V. Anisovich [c], C.A. Baker [a], C.J. Batty [a], D.V. Bugg [b], C. Hodd [b], H.C. Lu [b,1] V.A. Nikonov [c], A.V. Sarantsev [c], V.V. Sarantsev [c], B.S. Zou [b,1]

[a] *Rutherford Appleton Laboratory, Chilton, Didcot OX11 0QX, UK*

[b] *Queen Mary and Westfield College, London E1 4NS, UK*

[c] *PNPI, Gatchina, St. Petersburg district, Russia 188350*

Abstract

A combined fit is presented to data on $\bar{p}p$ annihilation in flight to final states $\eta\pi^0\pi^0$, $\pi^0\pi^0$, $\eta\eta$, $\eta\eta'$ and $\pi^-\pi^+$. The emphasis lies in improving an earlier study of $\eta\pi^0\pi^0$ by fitting data at nine $\bar{p}$ momenta simultaneously and with parameters consistent with the two-body channels. There is evidence for all of the $I = 0$, $C = +1$ $\bar{q}q$ states expected in this mass range. New resonances are reported with masses and widths (M, Γ) as follows: $J^{PC} = 4^{-+}$ $(2328 \pm 28, \Gamma = 240 \pm 90)$ MeV, 1^{++} $(1971 \pm 15, 240 \pm 45)$ MeV, 0^{-+} $(2285 \pm 20, 325 \pm 30)$ MeV, and 0^{-+} $(2010^{+35}_{-60}, 270 \pm 60)$ MeV. Errors on the masses and widths of other resonances are improved substantially. All states lie close to parallel straight line trajectories of excitation number v. mass squared. Small tensor and spin-orbit splitting is observed amongst $^3F_2$, $^3F_3$ and $^3F_4$ states.

[1] permanent address IHEP, Beijing 100039, China

Data from $\bar{p}p$ interactions in flight have the great merit of allowing a direct study of s-channel meson resonances R in formation reactions of the type $\bar{p}p \to R \to A+B$. Many decay channels A, B may be studied. Earlier, we have presented data on $\bar{p}p \to \eta\pi^0\pi^0$ [1], in which evidence was found for a number of $I = 0$ $C = +1$ mesons. That analysis fitted partial waves separately at each of nine $\bar{p}$ momenta; resulting magnitudes and phases were then interpreted in terms of resonances. Here our objective is to fit these data at all momenta simultaneously. The fit to resonance parameters is also made simultaneously to data on $\bar{p}p \to \pi^0\pi^0$, $\eta\eta$, $\eta\eta'$ and $\pi^-\pi^+$ reported earlier [2,3].

The resulting fit is constrained strongly by the requirement of consistency between all these channels and gives accurate determinations of masses and widths of most resonances found in the data. Fluctuations which were present in Refs. [1] at individual momenta are eliminated; this is particularly important in restricting phases to a smooth energy dependent behaviour. In the earlier work, fluctuations in the large high partial waves obscured details in small amplitudes, particularly low partial waves. We are now able to identify further resonances with $J^{PC} = 4^{-+}$, 1^{++} and 0^{-+}. The essential results of the new analysis are summarised by the masses and widths given in Table 1. These results supercede earlier determinations in Refs. [1] and [3]. The present paper completes our analyses of channels with $I = 0$, $C = +1$.

We begin by outlining the considerations which influence the form of our partial wave analysis. The first point is that the well-known $f_4(2050)$ appears strongly in all data sets, although we find a distinctly lower mass than that quoted by the Particle Data Group [4]. Its interferences with other partial waves determine their relative phases, which are found to vary little with mass. This requires that all partial waves follow a similar resonant behaviour to $f_4(2050)$. The way the $\eta\pi\pi$ analysis goes is that one immediately finds strong $J^{PC} = 3^{++}$ and 2^{-+} resonances. The two-body data require 2^{++} and 0^{++} resonances. Then, with increasing attention to detail, 4^{-+}, 1^{++} and 0^{-+} resonances emerge from the $\eta\pi\pi$ data.

We therefore parametrise each partial wave amplitude as a sum of resonances, plus a constant or slowly varying background where necessary. In analysing earlier data [1,3], we have found that resonances mostly cluster into two groups (a) from 1920 to 2050 MeV around $f_4(2050)$, (b) from 2220 to 2320 MeV, around $f_4(2300)$.

The background terms may parametrise t-channel exchanges. Singularities due to those exchanges are distant ($s \leq 1$ GeV^2), so it is to be expected that backgrounds will contribute mostly to low partial waves. This is what we find. The strong high partial waves with $J^{PC} = 4^{++}$ and 3^{++} are consistent with no background. In low partial waves ($J \leq 2$), the background is parametrised as a broad resonance or as a constant. Parametrising with resonances or constants guarantees that partial wave amplitudes obey the important constraint of analyticity, since a Breit-Wigner amplitude is analytic. This constraint plays a vital role in obtaining smooth phase variations. We see no evidence that strong threshold effects are present to perturb such a parametrisation.

Each partial wave amplitude then takes the form:

$$f = \sum_i \frac{g_i \exp(i\phi_i) B_i(\bar{p}p) B_i(AB)}{M_i^2 - s - iM_i\Gamma_i}. \tag{1}$$

The factors $B(\bar{p}p)$ and $B(AB)$ are standard Blatt-Weisskopf centrifugal barrier factors [5] which guarantee the correct threshold behaviour for each channel. A common radius for the centrifugal barrier is fitted to all partial waves. There is a strong optimum at 0.829 ± 0.021 fm. The full widths Γ_i of all resonances are taken to be constant because of the large number of open channels. Each resonance is fitted with a real coupling constant g_i and a phase ϕ_i.

We now discuss the channels fitted to the data. Fig. 1 shows mass projections on to $\pi\pi$ and $\eta\pi$ at two representative momenta and further figures are to be found in Refs. [1]. Histograms show the results of the present fit. In Ref. [1], final states fitted to $\eta\pi^0\pi^0$ data were dominantly $a_2(1320)\pi$, $f_2(1275)\eta$ and $\eta\sigma$, where σ stands for the $\pi\pi$ S-wave amplitude. There were small additional contributions from $a_0(980)\pi$, $f_0(975)\eta$ and $f_0(1500)\eta$. In the $\eta\pi$ mass projection at the higher beam momenta there is a distinct shoulder in the mass range around 1450 MeV. A fit to this part of the the mass spectrum and higher $\eta\pi$ masses requires further small contributions from $a_0(1450)\pi$ and $a_2(1660)\pi$. The evidence for $a_2(1660) \to \eta\pi$ is given in Ref. [6]. Parameters for $a_0(1450)$ are fixed to values of the PDG. However, evidence presented here for s-channel resonances does not depend significantly on these small $a_2(1660)\pi$ or $a_0(1450)$ contributions. We have tried including $f_0(1370)$ in the fit, but find negligible effect. It is known to decay weakly to $\pi\pi$ [7] compared with $f_0(1500)$, and the latter is already a small effect in the present data.

The 2-body channels $\pi\pi$, $\eta\eta$ and $\eta\eta'$ are related by SU(3), since π, η and η' are members of a single nonet. Formulae for these constraints are given in Refs. [3]. In outline, SU(3) allows $\eta\eta$ and $\eta\eta'$ amplitudes to be predicted from $\pi\pi$ using the well-known composition of η and η' in terms of $(u\bar{u} + d\bar{d})/\sqrt{2}$ and $s\bar{s}$, using the assumption that $\bar{p}p$ does not couple directly to $\bar{s}s$. The latter assumption has been tested in Refs. [3] and is well obeyed with one exception. The $f_0(2100)$ decays more strongly to $\eta\eta$ than to $\pi\pi$ by a factor 1.88; this compares with the SU(3) prediction of $0.8^4 = 0.42$. That is, the decay to $\eta\eta$ is a factor 4.5 stronger than predicted by the SU(3) relation. Since the $f_0(2100)$ is produced strongly, this feature suggests it has exotic character. Its coupling constants to $\pi\pi$, $\eta\eta$ and $\eta\eta'$ are therefore fitted freely.

For $\eta\pi\pi$, amplitudes for $a_2(1320)\pi$ and $f_2(1275)\eta$ are again in principle related by SU(2) constraints. These have been tried in the fit, but do not work well. This is probably because (a) there is a large mass difference between these channels and (b) the $f_2(1275)\eta$ threshold is close to the region we are analysing. Consequently, momenta in these channels are substantially different. This is likely to have large effects on matrix elements. We find it necessary to fit magnitudes and phases of $a_2(1320)\pi$ and $f_2(1275)\eta$ amplitudes freely.

Mass differences between π, η and η' also give rise to differences in momenta q in $\pi\pi$, $\eta\eta$ and $\eta\eta'$ channels, hence significantly different form factors and centrifugal barrier effects. We fit a form factor $\exp(-\alpha q^2)$ to all decays. The value of α optimises at 0.92 ± 0.10 GeV^{-2}.

We find that two minor improvements may be made to the fit. The phases ϕ_i of each resonance arise from multiple scattering in initial and final states, as explained in Ref. [8]. Firstly, to allow for overlap of resonances (hence departure from strict Breit-Wigner forms), phases ϕ_i are allowed to vary by up to $\pm 20^\circ$ for $\eta\eta$ and $\eta\eta'$ with respect to the $\pi\pi$ value. Secondly, we find significant improvements by allowing coupling constants g_i to vary for $\eta\eta$ and $\eta\eta'$ from their SU(3) values by factors constrained to the range 0.7 to 1.3. This probably reflects differences in form factors for different matrix elements. These refinements have only minor effects; without them conclusions on fitted resonance masses and widths change by only a few MeV.

For $J^P = 2^+$ and 4^+, $\bar{p}p$ may couple with orbital angular momentum $L = J \pm 1$ (e.g. $^3P_2$ and $^3F_2$). An ideal resonance should have the same phase for both L values (via multiple scattering through the resonance to each channel). We therefore take the ratio of coupling constants $r_J = g_{J+1}/g_{J-1}$ to be real. In fitting $\eta\pi\pi$ data, where a final state such as $f_2(1275)\eta$ may also have two or more L values, the ratio of coupling constant is likewise constrained to be real in initial fits. Again, we find small but significant improvements to the fit if these ratios for $f_2\eta$ and $a_2\pi$ decays are allowed to depart from real values by phase angles in the range up to $\pm 20^\circ$. But there is little effect on fitted masses and widths, merely a small improvement in the quality of the fit to data.

In Refs. [3], data on $\pi\pi$, $\eta\eta$ and $\eta\eta'$ required four $J^{PPC} = 2^{++}$ resonances. In addition, data on $\bar{p}p \to (\eta\eta)\pi^0$ provide evidence for a broad 2^+ $\eta\eta$ contribution with $M = 1980 \pm 50$, $\Gamma = 500 \pm 100$ MeV [9]. Central production of 4π provides even clearer evidence with the same mass and width [10]. We find that this broad component improves the present combined fit to $\eta\pi\pi$ and 2-body channels strongly. There is a clear optimum for the mass at $M = 2010 \pm 25$ MeV and for the width at 495 ± 35 MeV . Without this component, large interferences develop between the four 2^+ states, so as to simulate this broad contribution.

We have searched for ambiguous solutions by (i) removing each resonance (or background) one by one and re-optimising the rest, (ii) changing signs of amplitude ratios r and (iii) moving resonances in steps of 20 MeV in mass and 40 MeV in width over large ranges (9 steps each). Each iteration of the overall fit takes 10 minutes of computing and one solution converges in typically 20–50 iterations. So a large number of alternatives has been explored. All variants collapse back to the same solution.

Intensities of all fitted amplitudes are displayed in Fig. 2. Typical errors are $\pm 5\% - 10\%$ for the larger partial waves, increasing to $\pm 35\%$ for the smallest. Amplitudes which contribute less than 0.3% of the integrated cross section are found to change log likelihood by < 40 and are omitted.

Table 1 shows masses and widths of fitted resonances. Statistical errors are negligible, so quoted errors cover the range of solutions observed when components of the fit are varied. They include systematic changes when the radius of the centrifugal barrier is varied within its error. The last column of the Table shows changes in log likelihood when each component is removed from the fit to $\eta\pi^0\pi^0$ data and others are re-optimised. Our definition of log likelihood is such that it changes by 0.5 when one parameter changes by one standard deviation. For 2^+ and 4^+ components, there are also large changes in χ^2 arising in the fit to two-body data; those changes are close to values quoted in Refs. 3. Consequently, all of the components in the fit are highly significant.

The fit to $\pi\pi$, $\eta\eta$ and $\eta\eta'$ has changed little from that of Refs. [3], so attention will be concentrated here on fits to $\eta\pi\pi$. For those data there are some significant changes from the fit described in Refs. [1]. The origin of these changes is that ratios r of amplitudes with $L = J \pm 1$ are defined well by the two-body data, specifically by the polarisation data on $\bar{p}p \to \pi^-\pi^+$. Using these ratios in the combined fit introduces significant changes to 2^+ amplitudes in $\eta\pi\pi$. A knock-on effect is that there is also a large improvement in the fitted 3^+ amplitude towards the top of the mass range.

Argand diagrams are displayed in Fig. 3. Crosses mark individual beam momenta; Table 2 lists these beam momenta and the corresponding centre of mass energies. In many cases, one discerns in Fig. 3 that the amplitude varies rapidly in the low mass region and again in the high mass region. This indicates the presence of two resonances. However, for most partial waves, the phase variation with mass is fairly smooth. The data require a larger and more linear phase variation than can be produced by a single resonance. A sequence of resonances conspires to produce approximately a linear phase variation with mass squared s. In electronics, it is well known that a linear phase variation with frequency may be obtained with a Bessel filter [11], which has a sequence of poles almost linearly spaced in frequency. Meson resonances appear to behave in an analogous way as a function of $s = M^2$. Physically, such a system generates a time delay which is independent of frequency, since group velocity

J^{PC}	Mass M (MeV)	Width Γ (MeV)	r	$\Delta S(\eta\pi\pi)$
6^{++}	2485 ± 40	410 ± 90	0	245
4^{++}	2283 ± 17	310 ± 25	2.7 ± 0.5	2185
4^{++}	2018 ± 6	182 ± 7	0.0 ± 0.04	1607
4^{-+}	2328 ± 28	240 ± 90		558
3^{++}	2303 ± 15	214 ± 29		1173
3^{++}	2048 ± 8	213 ± 34		1345
2^{++}	2293 ± 13	216 ± 37	-2.2 ± 0.6	1557
2^{++}	2240 ± 15	241 ± 30	0.46 ± 0.09	468
2^{++}	2001 ± 9	312 ± 32	5.0 ± 0.5	168
2^{++}	1934 ± 11	271 ± 15	0.0 ± 0.08	1462
2^{++}	2010 ± 25	495 ± 35	1.51 ± 0.09	694
2^{-+}	2267 ± 14	280 ± 20		1349
2^{-+}	2030 ± 15	205 ± 20		
2^{-+}	1860 ± 15	250 ± 35		
1^{++}	2310 ± 60	255 ± 70		882
1^{++}	1971 ± 15	240 ± 45		1451
0^{++}	2337 ± 14	217 ± 33		
0^{++}	2102 ± 13	211 ± 29		
0^{++}	2040 ± 38	405 ± 40		
0^{-+}	2285 ± 20	325 ± 30		1342
0^{-+}	2010^{+35}_{-60}	270 ± 60		1189
5^{--}	2295 ± 30	235^{+65}_{-40}	0	
3^{--}	2300^{+50}_{-80}	340 ± 50	2.00 ± 1.1	
3^{--}	2210 ± 40	360 ± 50	-0.08 ± 0.23	
3^{--}	1982 ± 6	180 ± 35	0.006 ± 0.012	
1^{--}	2145 ± 50	270 ± 100	2.03 ± 1.25	
1^{--}	2000 ± 30	295 ± 85	1.05 ± 0.24	

Table 1
Resonances fitted to the data. Errors cover systematic variations observed in a variety of fits with different ingredients. The last column shows changes in $S = \log$ likelihood when each component is omitted in turn from the fit to $\eta\pi^0\pi^0$ data and remaining components are re-optimised.

is proportional to the gradient of phase v. frequency.

Beam momentum (MeV/c)	$\sqrt{s}$ (MeV)
600	1962
900	2049
1050	2098
1200	2149
1350	2201
1525	2263
1642	2304
1800	2360
1940	2409

Table 2
Momenta at which data are available and corresponding centre of mass energies.

We shall now comment on each J^P in turn, beginning with the high partial waves which are most conspicuous in the fit. For 4^+, the different peaks in Figs. 2(g) and (h) for $f_2(1275)\eta$ (full curves) and $a_2(1320)\pi$ (dashed) obviously demand two resonances. The lower resonance optimises at a mass of 2018 ± 6 MeV, considerably lower than the PDG average of 2044 ± 11 MeV. Our mass is determined by the maximum of the speed plot and is quite insensitive to the radius chosen for the centrifugal barrier. As the radius increases, all masses go up; however, for the error we find on the radius of the barrier, the contribution to the uncertainty on the mass is only 0.7 MeV. The width of the resonance does, however, correlate much more strongly with the radius, and this contributes an uncertainty to the width of 3.3 MeV. The $L = 3$ centrifugal barrier in the $\bar{p}p$ channel suppresses strongly the coupling of the lower 4^+ resonance to $f_2(1275)\eta$. The lower resonance couples purely to $\bar{p}p$ $^3F_4$, while the upper one requires a large $^3H_4$ component.

For $J^P = 3^+$, the different peaks in Fig. 2(d) for $f_2\eta$ (full curves) and $a_2\pi$ (dashed) again clearly demand two resonances. The Argand diagram of Fig. 3(h) also clearly demands two resonances. The upper resonance is considerably stronger in the present fit than in Refs. [1].

For $J^P = 2^+$, the $\eta\pi\pi$ data alone do not resolve $f_2(1934)$ and $f_2(2001)$ clearly, because both lie at the bottom end of the available mass range. One sees from Table 1 that removing the $f_2(2001)$ produces a change in log likelihood in $\eta\pi\pi$ data alone of only 168. This is because it may be interchanged to some extent with contributions from $f_2(1934)$. Here, the two-body data play a very important role, for two reasons. Firstly there are extensive data on the $\pi^-\pi^+$ channel down to 360 MeV/c, i.e. a mass of 1910 MeV. Secondly, the polarisation data provide a sensitive determination of the ratios of amplitudes between ${}^3F_2$ and ${}^3P_2$. The values of r_2 given in Table 1 are for ratios of coupling constants ${}^3F_2/{}^3P_2$, i.e. after factoring out the effect of the centrifugal barriers.

The earlier analysis of $\eta\pi\pi$ data [1] showed the requirement for three 2^+ states at 2020 ± 50, 2240 ± 40 and 2370 ± 50 MeV; the $f_2(1920)$ is known from data of GAMS [12] and VES [13]. These masses now adjust naturally by small amounts to those of Table 1. The lowest 2^+ state at 1934 MeV contributes strongly to $\bar{p}p \to \pi\pi$ and is dominantly ${}^3P_2$; that at 2001 MeV is largely ${}^3F_2$ and is close in mass to ${}^3F_3$ and ${}^3F_4$ resonances. The $f_2(2240)$ and $f_2(2293)$ are dominantly ${}^3P_2$ and ${}^3F_2$ respectively. Each of the Argand diagrams of Figs. 3(k) to (o) show at most a requirement for two 2^+ states. However, the two-body data require four 2^+ states, as reported in Refs. [3]. The $f_2(1934)$ lies below the available mass range for $\eta\pi\pi$ data.

We have speculated earlier on the possibility that the broad $f_2(1980)$ has a large component due to the 2^+ glueball [14,15]. In this context, its relative coupling to $\pi\pi$ and $\eta\eta$ is important. We fit these freely, with the result $g^2_{\eta\eta}/g^2_{\pi^0\pi^0} = 0.72 \pm 0.06$. This compares with the prediction 0.41 for $(u\bar{u} + d\bar{d})/\sqrt{2}$ and 1 for a glueball. The result lies midway between the two. In Ref. [3], the amplitude was expressed in terms of flavour mixing to a linear combination of states $\cos\Phi|u\bar{u} + d\bar{d} > /\sqrt{2} + \sin\Phi|s\bar{s} >$. With this parametrisation, the flavour mixing angle Φ optimises at $23.6 \pm 3.5^\circ$ compared with the value 35.6° for a glueball and 0° for $(u\bar{u} + d\bar{d})$. Some mixing between a glueball and neighbouring $q\bar{q}$ states is likely.

For $J^{PC} = 2^{-+}$, earlier data on $\bar{p}p \to \eta\pi^0\pi^0\pi^0$ demonstrate the presence of two states at 1860 and 2030 MeV [16]. The first of these states decays largely to $[f_2\eta]_{L=0}$ and the second decays weakly to this channel. The present $\eta\pi\pi$ data extend only down to 1960 MeV and therefore do not resolve these two states. We therefore fix their branching ratios between $f_2\eta$, $a_2\pi$ and $a_0\pi$ channels to the values of Ref. [16]. The $[f_2\eta]_{L=0}$ channel makes a dominant contribution to the 2^{-+} $\eta\pi\pi$ partial waves at low mass, see Fig. 2(c), full curve. The presence of a further η_2 at high masses is seen most clearly in ${}^1D_2 \to [f_2\eta]_{L=2}$, Fig. 2(c) chain curve; it is also visible in the smaller components $[a_0(980)\pi]_{L=2}$, Fig. 2(k) dashed curve and in ${}^1D_2 \to [f_0(1500)\eta]_{L=2}$, Fig. 2(k) chain curve. Its mass, 2267 ± 14 MeV, is somewhat lower than the earlier determination [1], 2300 ± 40 MeV. However, it agrees closely with a conspicuous peak observed [17] in the integrated cross section for $\bar{p}p \to \eta'\pi^0\pi^0$. There, a mass of 2248 ± 20 MeV is found and a width 280 ± 20 MeV. The latter determination of the width is better, so it is fixed at 280 MeV in the final fit to present data.

We now come to the new states. There is a well known ρ_5 ($\bar{q}q$ ${}^3G_5$) listed by the PDG at 2330 MeV. One expects a $q\bar{q}$ 4^{-+} state ($\bar{q}q$ $^1G_4$) of similar mass. We now observe small but well determined contributions from a 4^{-+} state at 2328 ± 28 MeV in $^1G_4 \to [a_2\pi]_{L=2}$, $[a_2\pi]_{L=4}$ and $[a_0\pi]_{L=4}$, Fig. 2(m). This resonance, although it contributes the smallest change in log likelihood in Table 1, is very stable throughout all fits. There is no doubt of its presence, despite the fact that it contributes only 2% of the integrated cross section. However, there is quite a large error on the width.

Next we consider 1^{++}. The earlier work of Ref. [1] found a strong $[a_2\pi]_{L=1}$ contribution near the $\bar{p}p$ threshold. In the new combined fit, the 1^{++} amplitude is large in several channels around 1975 MeV, falling rapidly at higher masses, see Fig. 2(j). Despite the fact that it lies at the bottom end of the available mass range, parameters of the resonance in this range are very stable: $M = 1971 \pm 15$ MeV, $\Gamma = 241 \pm 45$ MeV. Argand diagrams of Figs. 3(c) and (d) for $[f_2\eta]_{L=1}$ and $[\sigma\eta]_{L=1}$ require rapidly varying phases at low mass when one remembers that the amplitude goes to zero at the $\bar{p}p$ threshold; this rapid phase variation is a clear signature of the resonance.

At high masses, the phase variation observed in Refs. [1] suggested a 1^{++} resonance at 2340 ± 40 MeV with $\Gamma = 340 \pm 40$ MeV. We now find that a second 1^{++} resonance is definitely required. Without it, log likelihood is worse by 882; statistically this is a 25 standard deviation effect when one allows for the number of fitted parameters. Nonetheless, the mass of this resonance is the least well determined of all the resonances: $M = 2310 \pm 60$ MeV. The reason is that this resonance makes small contributions to the distinctive channels $a_2(1320)\pi$ and $f_2(1275)\eta$, and there are large interferences with the 0^- amplitude. As the resonance mass is changed, these interferences are able to absorb the variation with small changes in log likelihood. This resonance is most clearly visible in $[f_2\eta]_{L=1}$, Fig. 2(b), full curve.

Lastly we consider 0^{-+}. The $f_0(1500)\eta$ and $f_0(975)\eta$ channels, Fig. 2(i) (full and dotted curves) definitely require the presence of a high mass resonance with $M = 2285 \pm 20$ MeV. In addition, there is a very strong contribution close to the $\bar{p}p$ threshold in several channels of Figs. 2(a) and (i). A resonance is definitely required in this mass region. Without it, log likelihood gets worse by a very large amount, 1189. The effect of dropping it is illustrated by the dashed curves of Figs. 3(a) and (b). For this partial wave, amplitudes do not go to zero at the $\bar{p}p$ threshold, but instead go to values described by scattering lengths. It is not possible to exclude the possibility that the $\bar{p}p$ threshold plays a strong role (a cusp at the $\bar{p}p$ threshold). This makes the identification of the mass of the lower resonance difficult. The optimum is at 2010^{+35}_{-60} MeV.

There is just one significant change in the fit to two-body data, compared with Refs. [3]. There is a strong 3^{--} resonance in the low mass range. It interferes strongly with 2^{++} states in data on $\bar{p}p \to \pi^-\pi^+$. Small changes in the masses and widths fitted to the 2^+ states have had the effect of increasing the mass of this ρ_3 from 1960 ± 15 MeV [3] to 1982 ± 6 MeV; the fitted width has also increased slightly.

Fig. 4 illustrates the quality of the fit at two momenta. It shows the angular distributions for production of mass regions centred on (a) and (d) $f_2(1275)$, (b) and (e) $a_2(1320)$, (c) and (f) $a_0(980)$. In all cases, there are background contributions below these resonances, particularly in the case of the small $a_0(980)$ signal. The angular distributions are well reproduced by the fit in all cases.

We now turn to the interpretation of the results. Fig. 5 shows plots of mass squared v. excitation for all J^P; in making this plot, we use the K-matrix mass of 1598 MeV for $f_2(1565)$ [19], and 1400 MeV for $f_0(1370)$ [7]. A remarkably simple pattern is apparent in Fig. 5. All states lie close to parallel straight-line trajectories. These trajectories extrapolate well to known states in the mass range 1200–1700 MeV. [We do not, however, attempt to place the η on the 0^- trajectory, since its mass is affected strongly by the instanton interaction]. The simplicity of Fig. 5 suggests that observed states are $q\bar{q}$ rather than hybrids. Using PDG masses for resonances below 1.9 GeV, the mean slope of the trajectories is 1.143 ± 0.013 GeV^2 per excitation. The most accurate determination of the slope comes from the $^3P_2$ trajectory, which begins with the well known $f_2(1275)$. However, one must expect some deviations from straight lines due to local perturbations, for example (a) from mixing with nearby glueballs or hybrids, (b) from level repulsion between 2^+ states, (c) from nearby thresholds, particularly in the low mass region, and (d) from variation with s of the effects of tensor and spin-orbit splitting. The 0^+ trajectory is drawn with $n = 1$ for $f_0(1370)$. The line does, however, go through $f_0(980)$, and it is possible that this state is the $n = 1$ ground state rather than a molecule.

In the absence of tensor and spin-orbit splitting, $^3F_4$, $^3F_3$ and $^3F_2$ states are degenerate in mass. Tensor and spin-orbit splitting may be assessed from the relations [18]

$$\Delta M_{LS} = [-20M(^3F_2) - 7M(^3F_3) + 27M(^3F_4)]/54, \quad (2)$$

$$\Delta M_T = [-4M(^3F_2) + 7M(^3F_3) - 3M(^3F_4)]/14. \quad (3)$$

For both multiplets of Table 1, $^3F_3$ states lie highest in mass, requiring significant tensor splitting. This splitting is in the sense predicted by one-gluon exchange. Using a linear confining potential at large r plus one-gluon exchange at small r, Barnes et al. [20] predict $\delta M_T = 15$ MeV for the lower multiplet. From Table 1, one finds $\delta M_T = 20 \pm 4.5$ MeV for the lower multiplet and 7.1 ± 7.3 MeV for the upper one; errors take into account observed correlations in fitted masses. Because we use the same centrifugal barrier for $^3F_4$, $^3F_3$ and $^3F_2$ states, there is almost no correlation with the radius of the barrier.

Results are consistent with the prediction from one-gluon exchange, though the error is sizable. Presently the spin-orbit splitting cannot be predicted accurately. Observed splittings are $\delta M_{LS} = 2.4 \pm 4.4$ MeV for the lower multiplet and -6.3 ± 5.1 MeV for the upper one; these average approximately to zero.

In summary, the expected $q\bar{q}$ states in this mass range are observed with well determined masses and widths, except for the lower 0^- and the upper 1^+ state. They follow a simple pattern requiring linear trajectories of mass squared against excitation number, with a slope of 1.143 ± 0.013 GeV^2 per excitation. In addition, there is evidence for a broad 2^+ component with $M = 2010 \pm 25$ MeV, $\Gamma = 495 \pm 35$ MeV. Tensor splitting for ^3F states is, within sizeable errors, consistent with that predicted from one-gluon exchange and a linear confining potential. Spin-orbit splitting of ^3F states is consistent with zero.

1 Acknowledgement

We thank the Crystal Barrel Collaboration for allowing use of the data. We acknowledge financial support from the British Particle Physics and Astronomy Research Council (PPARC). We wish to thank Prof. V. V. Anisovich for helpful discussions. The St. Petersburg group wishes to acknowledge financial support from PPARC and INTAS grant RFBR 95-0267.

References

[1] A.V. Anisovich et al., Phys. Lett. B452 (1999) 173; Nucl. Phys. A651 (1999) 253.

[2] A.V Anisovich et al., Phys. Lett. B468 (1999) 304 and 309; Nucl. Phys. A662 (2000) 344.

[3] A.V Anisovich et al., Phys. Lett. B471 (1999) 271; Nucl Phys. A662 (2000) 319.

[4] Particle Data Group (PDG), Euro. Phys. Journ. 3 (1998) 1.

[5] D.V. Bugg, A.V. Sarantsev and B.S. Zou, Nucl. Phys. B471 (1996) 59.

[6] A. Abele et al., Euro. Phys. J. C8 (1999) 67.

[7] A.V. Anisovich et al., *Resonances in* $\bar{p}p \to \eta\pi^+\pi^-\pi^+\pi^-$, submitted to Nucl. Phys. A.

[8] V. V. Anisovich, D.V. Bugg, A.V. Sarantsev and B.S. Zou, Phys. Rev D50 (1994) 1972.

[9] A.V Anisovich et al., Phys. Lett. B449 (1999) 154.

[10] D. Barberis et al., Phys. Lett. B471 (2000) 440.

[11] H. Baher, *Analog and Digital Signal Processing*, (Wiley, Chichester, 1990), p243.

[12] D. Alde et al., Phys. Lett. B241 (1990) 600.

[13] G.M. Beladidze et al., Zeit. Phys. C54 (1992) 367.

[14] D.V. Bugg and B.S. Zou, Phys. Lett. B396 (1997) 295.

[15] D.V. Bugg, *Resonances around 2 GeV: $q\bar{q}$ and glueballs*, Hadron99 Proceedings (to be published).

[16] A.V Anisovich et al., Phys. Lett. B477 (2000) 19.

[17] A.V Anisovich et al., *Data on $\bar{p}p \to \eta'\pi^0\pi^0$ for masses 1960 to 2410 MeV*, submitted to Phys. Lett. B.

[18] C.A. Baker et al., Phys. Lett. B467 (1999) 147.

[19] D.V. Bugg et al., J. Phys. G: Nucl. Phys 4 (1978) 1025.

[20] T. Barnes, private communication.

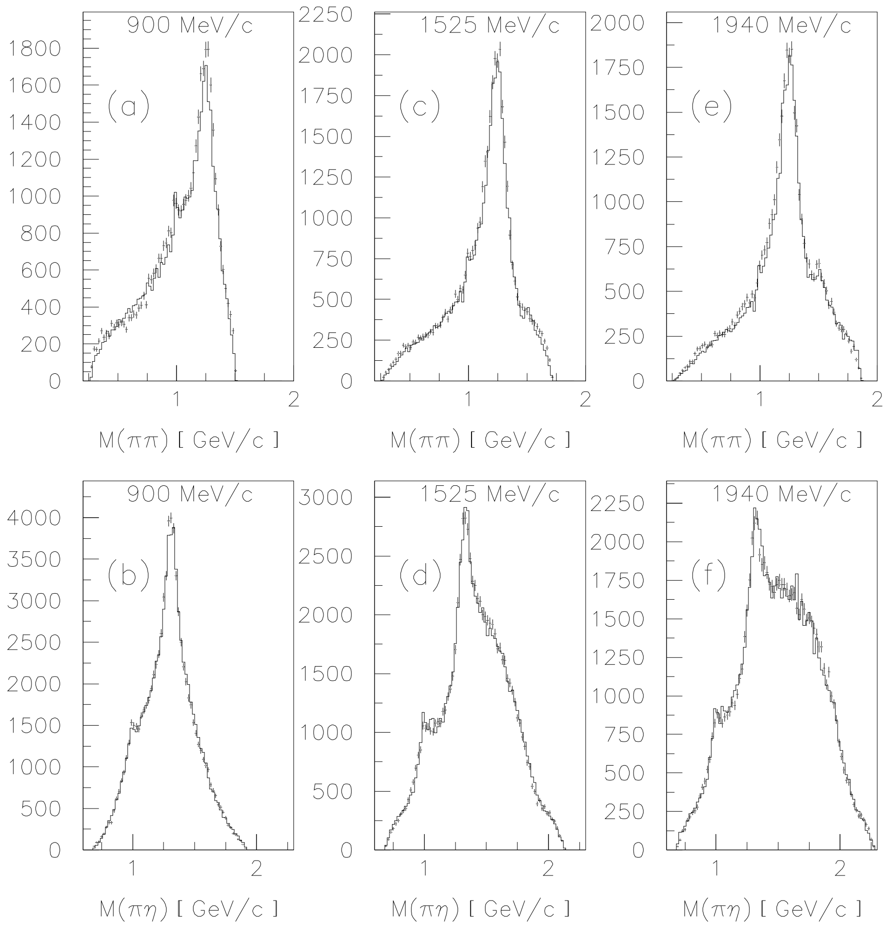

Fig. 1. Mass projections on to $M(\pi\pi)$ and $M(\pi\eta)$ for data at (a) and (b) 900 MeV/c, (c) and (d) 1525 MeV/c, (e) and (f) 1940 MeV/c; histograms show the result of the fit.

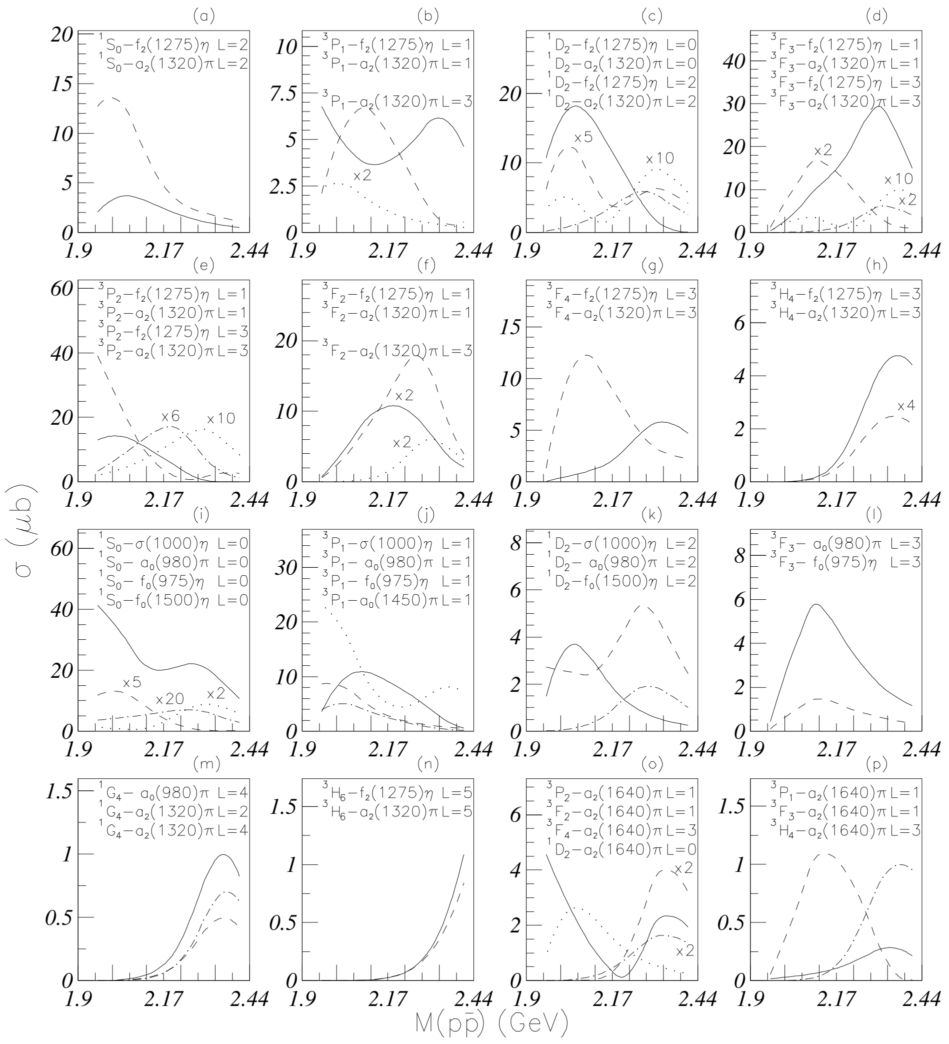

Fig. 2. Intensities fitted to individual partial waves. The titles in each panel indicate in descending order full, dashed, chain and dotted curves; $\sigma(1000$ denotes the broad σ $(f_0(400-1200))$ in the $\pi\pi$ amplitude. Numerical values indicate factors by which small intensities have been scaled so as to make them visible.

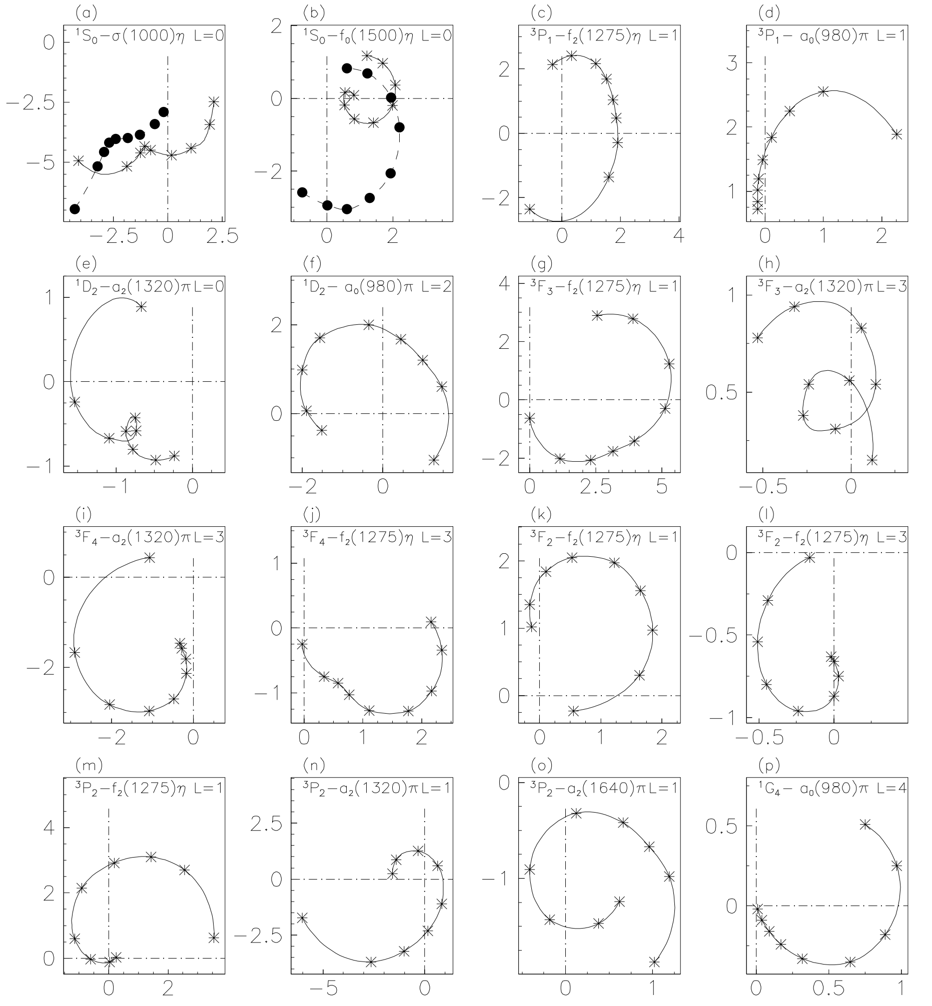

Fig. 3. Argand diagrams for prominent partial waves; for (a) and (b), dashed curves show the effect of removing the lower 0^- resonance. Crosses mark beam momenta of Table 2; in all cases, the amplitude moves anti-clockwise with increasing beam momentum.

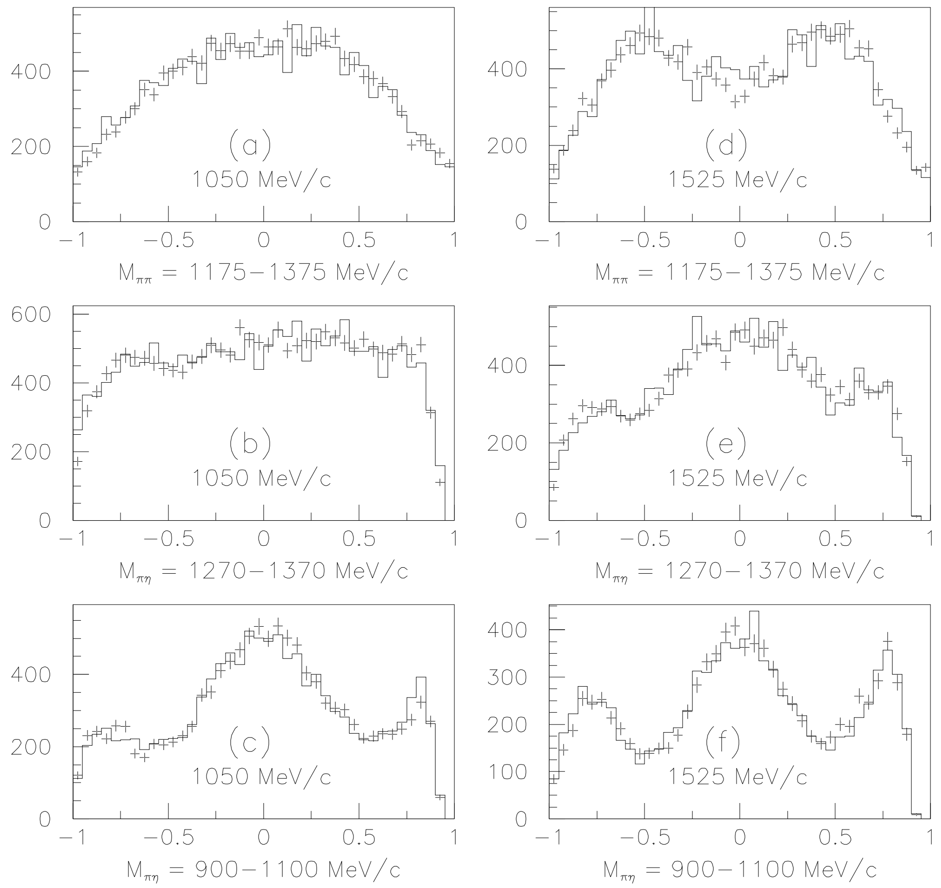

Fig. 4. Centre of mass angular distributions for production of (a) $f_2(1275)\eta$, (b) $a_2(1320)\pi$, (c) $a_0(980)\pi$ at 1050 MeV/c; (d)-(f) show corresponding angular distribtuions at 1525 MeV/c. Histrograms show the fit.

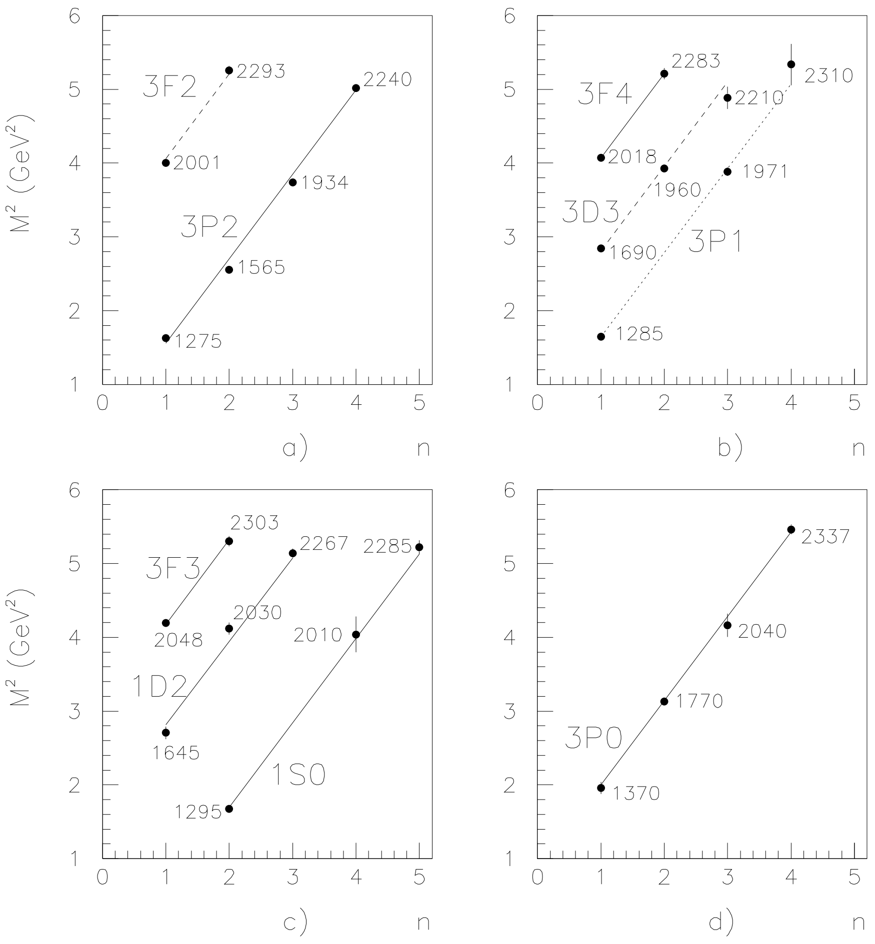

Fig. 5. Plots of M^2 v. radial excitation number, n. Straight line trajectories are drawn in all cases with a slope of 1.143 GeV^{-2}.